Friction, Fracture, and Earthquakes

Eric G. Daub[1,2] and Jean M. Carlson[1]

[1]Department of Physics, University of California, Santa Barbara

[2]Geophysics Group and Center for Nonlinear Studies,

Los Alamos National Laboratory

Abstract

A primary goal in seismology is to identify constraints arising from the small scale physics of friction and fracture that can provide bounds on seismic hazard and ground motion at the fault scale. Here we review the multi-scale earthquake rupture problem and describe a physical model for the deformation of amorphous materials such as granular fault gouge. The model is based on Shear Transformation Zone (STZ) Theory, a microscopic model for plastic deformation. STZ Theory ties fault weakening to the evolution of an effective temperature, which quantifies configurational disorder and captures the spontaneous formation and growth of narrow shear bands in the fault gouge.

1 Introduction

Earthquakes occur due to an instability in the deformation of rocks in the earth's crust. A schematic illustration of a fault is given in Figure 1 (left). The two sides of the fault are driven laterally, in opposite directions, characteristic of a strike-slip fault. Due to large temperatures and pressures, rocks deep in the earth, red in the illustration, flow at rates of order cm/year, like a highly viscous fluid, driving the motion of tectonic plates comprising the earth's crust. At shallower depths (0-15 km), blue in Figure 1, and referred to as the seismogenic zone, rocks resist plate motion, and remain locked until the force becomes large enough that the material fails, and the fault slips rapidly on the order of meters/second in an earthquake.

However, faults are more complex than simple planar surfaces where rocks slide past each other. The fault interface is also filled with crushed pieces of rock called gouge, and the basic contact interactions between the particles dictate how the gouge

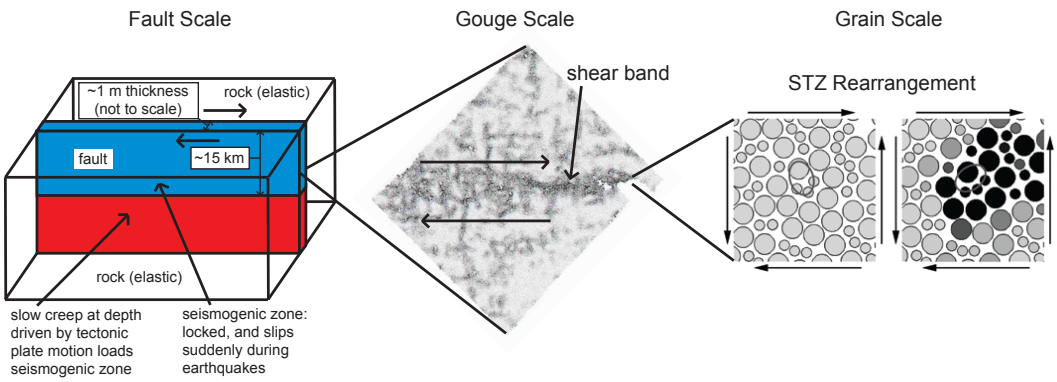

Figure 1: Diagram illustrating the multi-scale nature of the earthquake rupture problem. The system progressively decreases in scale from left to right. (left) Fault scale, with a thin layer of fault gouge sheared between elastic rocks. (center) Deformation within the fault gouge, where a shear band that is much narrower than the gouge thickness accommodates plastic strain in the gouge. Shear band image taken from Falk and Shi [1] and reoriented to match the sense of shear of the fault and grains. (right) Individual rearrangements occur at the grain scale and produce plastic strain in the fault gouge. The left grain scale picture shows a "positive" STZ orientation, and as the grains are sheared the gouge deforms plastically and the particles change to a "negative" orientation in the right grain picture. STZ diagram taken from Falk and Langer [2] (Reprinted with permission. Copyright 1998 by the American Physical Society. http://link.aps.org/abstract/PRE/v57/p7192).

deforms in response to large tectonic stresses. In Figure 1 the deformation of the gouge (right) determines the frictional properties of the interface (center), which controls rupture propagation along the fault (left) that is many kilometers long.

Because earthquakes occur deep in the crust, the physical and dynamical properties of faults, such as stress, strain, friction, geometry, slip velocities, and rupture propagation speeds, cannot be observed directly. Instead scientists rely on a variety of complementary methods, including geologic, seismic, and geodetic observations, experiments on laboratory scale faults, and theoretical and numerical studies. Together, these methods provide a basis for analysis of individual earthquakes after they occur, as well as forward modeling (often in simplified settings) to identify cause and effect relationships between friction and material properties and the resulting dynamics, that may help constrain estimates of the range of future behavior which may occur. This latter approach defines the emerging interdisciplinary field

of earthquake physics, which aims to connect geophysics, material science, laboratory studies, and seismic observations to reduce uncertainties in seismic hazard – e.g., earthquake magnitude, frequency, ground motion, and attenuation – based on understanding of the physics of the source. In this review, we focus primarily on theoretical and numerical results of dynamic earthquake rupture across multiple length scales, from grains up to faults. The modeling results capture phenomena which are observed in the laboratory and in the earth – e.g., plasticity, shear localization, and crack-like, pulse-like, and supershear ruptures – and we discuss how numerical simulations with physical friction parameters relate to important results from seismic and laboratory observations of earthquakes and faulting.

In Sections 2-5 we review constitutive laws, plasticity, strain localization, and dynamic rupture, drawing on results from physics, geology, materials science, and engineering. In Section 6 we describe recent work in which deformation and dynamics are spatially resolved within the gouge layer and on the scale of the fault. This grain-scale model reduces the nonequilibrium statistical mechanics of a collection of densely packed particles to a description characterized by deforming, local shear transformation zones (STZs). STZ Theory has been applied to a wide range of dense, disordered solids and captures features from both experiments and numerical studies, including dynamic formation of shear bands. Here the STZ model acts as a friction law in fault scale numerical simulations of dynamic earthquake rupture and places physical constraints on fault scale slip and ground motion.

2 Constitutive Laws

Modeling dynamic earthquake rupture at multiple scales requires new tools that incorporate the essential physics at each scale. At the fault scale, this includes the elastic response of the rock and the varying elastic properties in the velocity structure. Other effects such as plastic yielding and off-fault damage are often included. The challenge is to account for small scale physical processes, while maintaining resolution at the fault scale. Traditionally, this is accomplished using a friction law. These relations, also known as constitutive laws, are often motivated by laboratory experiments, and determine the shear stress on the fault, usually dependent on quantities such as the slip, slip rate, or other dynamic variables quantifying the internal state. Earthquakes occur at extreme physical conditions, including high pressures and temperatures, generating large amounts of slip at high slip rates. All current experimental data compromises on at least one of aspect of the physics of the source.

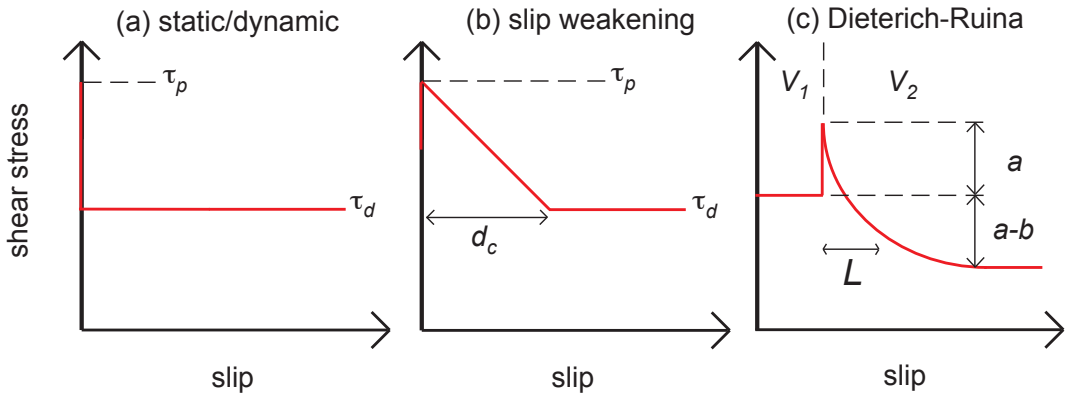

Figure 2: Friction laws for earthquake faults. (a) Static/dynamic friction, (b) linear slip weakening, and (c) Dieterich-Ruina Rate and State law in a velocity step experiment.

2.1 Univariate Relationships

The simplest example of a friction law is static/dynamic friction illustrated in Figure 2 (a). The shear stress $\tau = \sigma\mu$ is proportional to the normal stress σ, and the proportionality constant is μ (the static μ_s or dynamic μ_d coefficient of friction). The instantaneous stress change from the peak value to the sliding value is unphysical. Seismologists have proposed many modifications to static/dynamic friction to fix this problem.

Slip-weakening (SW) laws [3, 4, 5, 6, 7] have been used extensively to study dynamic rupture [4, 5, 8, 9, 10]. Shear stress τ is a decreasing function of slip u up to some slip-weakening distance d_c, beyond which a constant stress is prescribed. The most common form is piecewise linear. The fault is initially locked. Shear stress increases to the peak stress τ_p before initiating slip, and then weakens as the fault slips (Fig. 2 (b)). Stress is a fixed function of slip, which sets the amount of energy lost to fracture and frictional dissipation (the area under the curve plotting shear stress as a function of slip). Because the sliding stress τ_d is constant, the fault cannot regain strength once it ruptures.

A common practice in engineering applications is to measure the slip rate dependence of friction, which leads to a friction law called the Stribeck curve [11]. Like slip-weakening, this friction law depends on a single quantity. However, purely velocity dependent friction fails to capture the stress drop required to propagate dynamic

rupture (the stress at onset must be greater than the stress at termination) as well as stiffness dependence of laboratory observations of the transition between stick slip and steady sliding [12].

2.2 Rate and State Friction

The Dieterich-Ruina (DR) law is a phenomenological friction law, introduced to capture experimental observations of both steady state velocity dependence and transient slip and time dependence of friction [13, 14], and is defined in terms of rate (velocity V) and a single dynamic state variable θ. The shear stress τ depends on both rate and state logarithmically in the DR law:

$$\tau = \sigma \left[f_0 + a \log \left(\frac{V}{V_0} \right) + b \log \left(\frac{\theta V_0}{L} \right) \right]. \tag{1}$$

Other parameters include normal stress σ, constants a and b determining the rate and state dependence, length scale L, and reference friction coefficient and slip velocity, f_0 and V_0, respectively.

A dynamic equation determines how θ evolves. The ageing equation [15]

$$\frac{d\theta}{dt} = 1 - \frac{\theta V}{L} \tag{2}$$

is most common, and captures experimentally observed frictional strengthening with time which occurs when the surfaces are at rest. θ has dimensions of time and is often interpreted as the lifetime of surface asperity contacts, which is consistent with experiments by Dieterich and Kilgore [16] that imaged the dynamic evolution of contact area between sliding surfaces at various slip rates.

Alternative forms for the state equation have been proposed based on other laboratory data. The most common is known as the slip law [15], in which the state variable evolves only if the surfaces are sliding. The ageing law fits data better for rock healing, while the slip law fits data better for the frictional response to a velocity step. A composite law was proposed by Kato and Tullis [17] to combine the advantages of the ageing law for healing and the slip law for rapid changes in sliding.

The role of the parameters in Eq. 1 are best understood through a velocity step experiment, illustrated in Figure 2 (c) [18]. An interface is sheared at a constant slip rate V_1, and reaches steady state. The slip rate is then suddenly increased to $V_2 > V_1$, and the friction evolves to a new value over a length scale L. There is a transient increase in the friction, with a magnitude of a. The change in the steady state friction is $(a - b)$. If $a > b$, the friction is rate strengthening. If $a < b$, the friction is

rate weakening. Unstable rupture only occurs with rate weakening parameters [12]. Laboratory experiments show that a and b vary with temperature [19, 20, 21, 22], indicating that the frictional rate dependence varies with depth.

The logarithmic rate dependence of the DR law is problematic at $V = 0$. Several regularizations have been proposed. These include adding a small cutoff velocity to the slip rate [23, 24] and changing the logarithm to an inverse hyperbolic sine [25]. The need to regularize the DR laws underscores the fact that the law is phenomenological. In contrast, the STZ friction law described in Section 6 is derived from physical processes acting at smaller scales and thus provides quantitative estimates for cutoffs, crossovers, and limiting behavior at small times, lengths, and velocities.

Another problem with the DR law is that the experiments it is based on differ greatly from the conditions in the earth's crust. Seismic slip rates are on the order of meters/second, while the experiments that led to the development of the DR law range from microns/second to millimeters/second [13]. Laboratory experiments at seismic slip rates show that friction is much lower than the values predicted by extrapolation of the logarithmic weakening in DR friction [26, 27, 28, 29, 30, 31, 32, 33]. Low friction coefficients at seismic slip rates have important implications for the strength of faults [34, 35], the energy balance of faulting [36], and fault slip in dynamic rupture models [37, 38, 39].

3 Plasticity in Amorphous Materials

An alternative approach to laboratory based, phenomenological friction begins with the physics of how amorphous materials such as fault gouge deform and fail. Amorphous materials are composed of particles (grains, atoms, bubbles, molecules) that are arranged so that their centers of mass are disordered. Under certain conditions, these materials behave like solids – small deformations are elastic (shear stress is proportional to the shear strain), the material exhibits a yield stress, and is "jammed." Other conditions produce dynamics more like a fluid – the shear stress depends on the strain rate instead of the strain, and the material flows. One example is sand which supports the static load of a person standing on the beach, but also flows through his/her fingers.

Deformation of a collection of particles breaks down into two components – the uniform, elastic (affine) component which is the same for all the particles, and heterogeneous, plastic (non-affine) component, describing deviations from the average. Affine displacements produce the linear, elastic response. Non-affine deformation requires new models to describe the material properties.

Molecular dynamics or discrete element simulations are frequently used to study

the dynamics of amorphous materials [2, 40, 1, 41, 42]. A simulation of a glass is shown in the center of Figure 1 [1]. The material is under tensile strain, but the deformation results in shear deformation (indicated by the arrows). The dark regions show where non-affine deformation occurs. The plastic deformation is localized to a narrow shear band, a common mechanism of failure in amorphous materials.

While simulations provide insight into how these materials deform, they are not efficient for studying larger scale behavior. Instead, physicists are working to develop a continuum model to describe the deformation of amorphous materials, much like continuum mechanics describes solids and Navier-Stokes describes fluids.

Molecular dynamics simulations show that plastic deformation occurs when localized regions rearrange from one metastable configuration to another [2, 40]. A picture of one of these regions is shown at the right in Figure 1. These zones are known as Shear Transformation Zones (STZs), and STZ theory captures many features of experiments such as a yield stress and fracture in glasses [2, 40], boundary lubrication [43], granular flow [41], shear band formation in glassy materials [44, 45], dynamic earthquake rupture [38], strain localization in dynamic earthquake faulting [46, 47, 48], and laboratory stick-slip [49]. As the particles are sheared, the ellipse drawn through the center of the particles flips its orientation. STZs are created and annihilated as energy is dissipated in the system, whereby the material accumulates plastic strain. Instead of simulating every single particle in the system, it is sufficient to capture the deformation by tracking the number of STZs and how frequently they flip. To do this the theory requires a quantity that characterizes the internal degrees of freedom.

Statistical mechanics provides a good description of equilibrium systems, but when large numbers of particles are actively provided with energy, these tools break down. Energy supplied to shear amorphous materials is dissipated as the material flows, and these systems are frequently stuck in a metastable disordered state. The thermal temperature does not characterize fluctuations in the internal state, and in the case of granular materials and other athermal systems, the thermal temperature can be completely irrelevant.

One idea for a state variable for amorphous materials is known as effective temperature [50]. In thermodynamics, temperature T is defined based on the partial derivative of the entropy S with respect to the internal energy E:

$$\frac{1}{T} = \frac{\partial S}{\partial E}. \tag{3}$$

The energy in this case is the internal energy of the individual constituents of the system. The effective temperature T_{eff} is defined by the partial derivative of the

entropy S with respect to the potential energy U of the packing:

$$\frac{1}{T_{eff}} = \frac{\partial S}{\partial U}. \tag{4}$$

The idea is that the disorder relevant to deformation in contained in the packing of the system and not in in the kinetic degrees of freedom, and thus the effective temperature better describes the internal state of an amorphous material than the thermal temperature.

STZs are regions that are susceptible to plastic deformation because they are more disordered. An elevated effective temperature means that locally there are more STZs. This general aspect of the small scale physics of deformation in amorphous materials can be accounted for in dynamic earthquake rupture simulations by using STZ Theory and effective temperature [50] to describe friction in the gouge layer (Section 6).

4 Strain Localization

Strain localization occurs when deformation is restricted to a narrow band rather than distributed uniformly throughout a material. Figure 3 plots the flow profile (top) and the strain rate profile (bottom) for (a) homogeneous and (b) localized deformation in simple shear. Homogeneous flow is the expected flow profile for a Newtonian Fluid. In localized flow there is a peak in the strain rate profile, which defines the shear band, and the material above and below move intact with the boundaries.

Numerical simulations [51] of sheared gouge with a distribution of particle diameters produces results similar to the glassy material shown in Figure 1 (center) [1]. Deformation localizes to a region narrow relative to the gouge width. Localization is also observed in laboratory experiments [52, 53, 54, 55, 56, 57, 58, 59] and field observations of exhumed faults [60, 61, 62]. An exhumed fault was formerly at seismogenic depths, where it experienced many earthquake cycles. Through uplift and erosion it rises to the surface. Observations of exhumed faults indicate that most of the deformation is localized to a narrow shear band, also known as a prominent fracture surface, within the fault zone. Figure 4 illustrates the observed features of the fault core of the Punchbowl Fault in Southern California [61]. Similar observations were made on the Median Tectonic Line in Japan [62].

Localization does not occur for all fault zones, as demonstrated by observations from the San Andreas Fault Observatory at Depth (SAFOD) project [63]. The

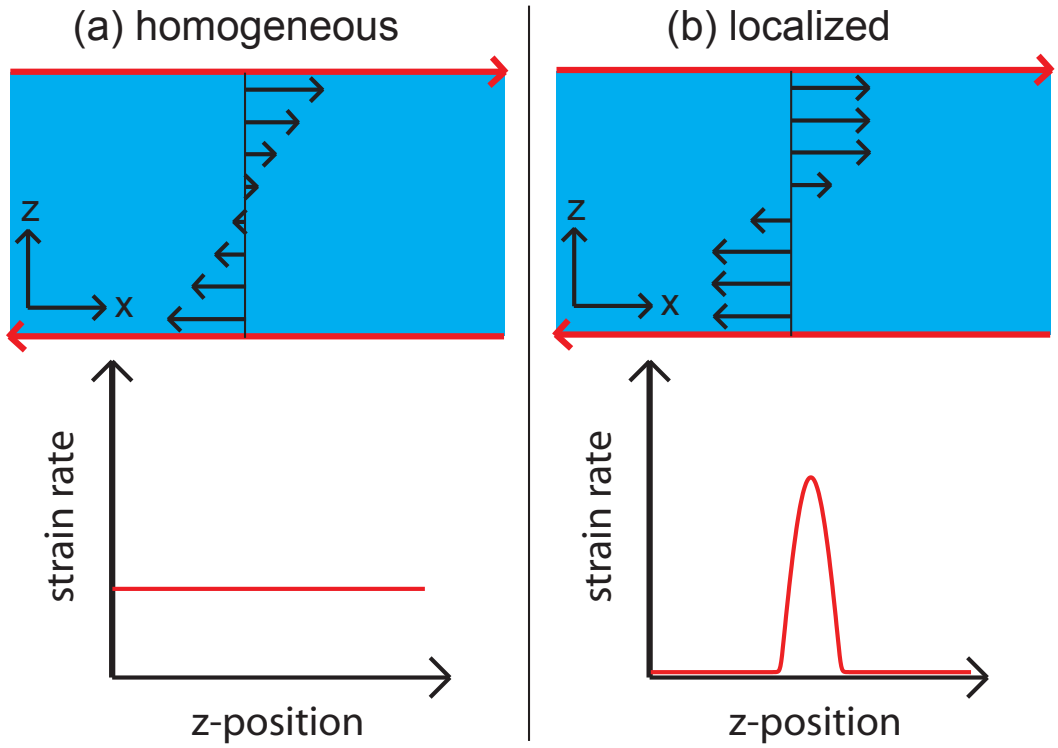

Figure 3: Illustration of homogeneous and localized deformation in amorphous materials. The upper pictures show the flow profile in the material, and the lower picture shows the strain rate as a function of position. In (b) the peak strain rate coincides with the center of the shear band.

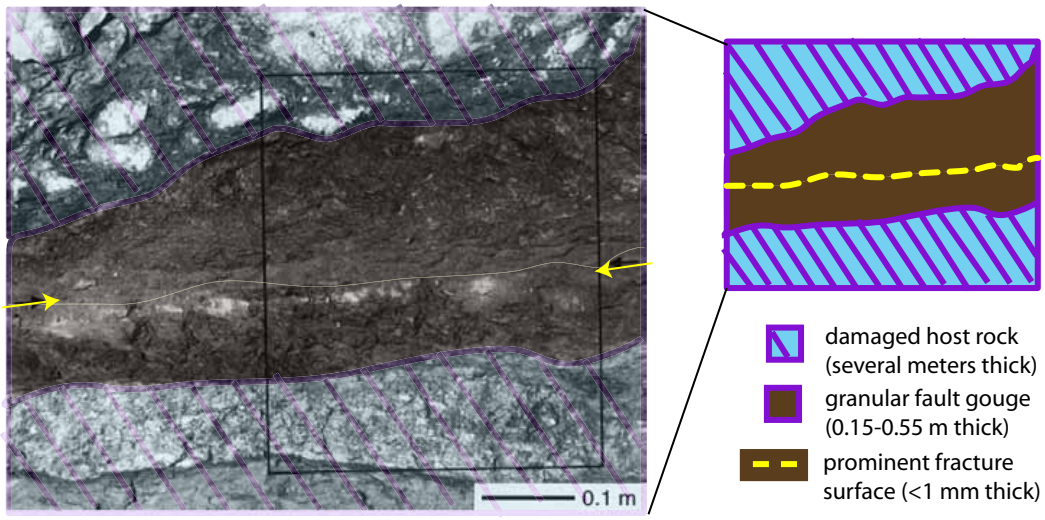

Figure 4: Field observations from an exhumed fault. The fault contains a layer of a finely crushed fault gouge (dark material), and the slip in the gouge is localized in a narrow shear band (yellow arrows). Figure adapted from Chester and Chester [61]. (Reprinted with permission. Copyright 1998 by Elsevier.)

SAFOD observations involve drilling through the actively creeping portion of the San Andreas Fault near Parkfield, CA. Samples of the fault zone show no fracture surface or other localized deformation within the gouge for this segment of the San Andreas [64]. Instead, the core samples show that deformation occurs throughout two gouge layers that are each a couple of meters thick.

5 Dynamic Earthquake Rupture

At the fault scale, ruptures propagate in space and time when tectonic loading generates a frictional instability. Individual faults are approximated by some average stress, geometry, and material characteristics. Heterogeneities also play an important role in dynamic rupture. In this review, we focus primarily on examples of ruptures propagating along interfaces with essentially uniform material properties and initial conditions in order to isolate the dynamical impact of friction and localization. Simple ruptures have been used to study the role of friction laws in earthquake dynamics (e.g., [65, 66, 67, 68, 23, 38, 39]), while many other studies of earthquake dynamics have focused on complexity of earthquake rupture, including complexity of individual ruptures (e.g., [69, 70, 71, 72, 73, 74, 75, 76]) and spatiotemporal complexity in sequences of earthquake ruptures (e.g., [77, 78, 79, 80, 81]).

Ruptures are modeled by solving for the elastodynamic response of two large blocks of rock governed by a friction law at their interface. The fault is loaded with an initial shear stress, and rupture is initiated by overstressing the stress on a small patch. The simulation solves for the spontaneous propagation of slip along the fault, and the resulting ground motion generated at the earth's surface.

Three examples of rupture propagation in dynamic earthquake simulations with STZ friction (Section 6) are shown in Figure 5. In each case, the friction and stress characteristics are taken to be homogeneous, aside from the nucleating patch in the center and the absorbing barriers on the edges. The simulations show the evolution of slip rate as a function of space and time.

The slip within the initiating patch grows in time until sufficient slip has accumulated to increase the stress at neighboring fault patches and causes them to slip. In Figures 5(a)-(c), nucleation lasts about 0.4 s, after which the ruptures spontaneously propagate out to the edges of the fault. The rupture velocity (of order km/s) is the inverse slope of the lines propagating out from the nucleation site, while the slip rate (of order m/s) is given by the color scale. The slip rate as a function of time for any given point along the fault is obtained by taking a vertical slice of the figure, whereas the slip rate as a function of position at a fixed point in time correspond to a horizontal slice.

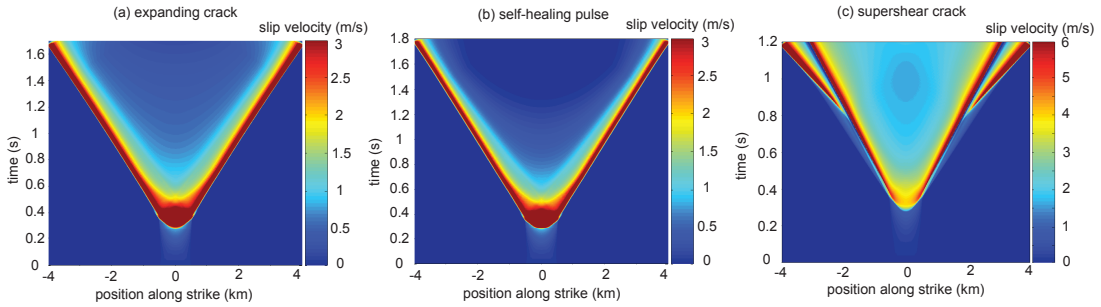

Figure 5: Dynamic rupture propagation in space and time for (a) expanding crack, (b) self-healing pulse, and (c) supershear ruptures. Rupture nucleates at the center of the fault, and the rupture spontaneously grows until it encounters a barrier at the edge of the fault. These simulations use the STZ friction law (Section 6) and stress conditions are homogeneous aside from the nucleating patch. Crack-like rupture propagation occurs at intermediate values of the shear stress. Self-healing pulses occur for low values of the initial shear stress. Supershear rupture occurs at high stresses and small frictional length scales.

Dynamic rupture modeling has revealed that the form and speed of rupture propagation have a significant impact on ground motion. The different forms – crack, pulse, and supershear – are illustrated in Figure 5.

Many dynamic rupture simulations produce crack-like ruptures [82, 4, 5, 9]. In an expanding crack (Figure 5(a)), the earthquake initiates at the hypocenter and propagates bi-laterally until it reaches the fault boundaries or strong patches that it is unable to break. Only then does the rupture arrest (this phase is not shown in the figure), collapsing in from the boundaries, so that that the hypocenter slips for the entire duration of the earthquake. Ruptures with slip-weakening friction usually produce crack-like slip profiles due to the lack of healing in the constitutive model. The rupture front approaches a limiting speed (slightly less than the shear wave speed), and the largest slip rate (shown as red on the slip rate scale) occurs right behind the rupture front where strain energy is released rapidly from the elastic bulk.

Alternatively, Figure 5(b) shows the slip rate as a function of position for a self-healing pulse. The rupture propagates out from the nucleation point and the peak slip rate occurs right behind the rupture front as for the expanding crack, but in this case the fault heals shortly after slipping, so that each point along the fault slips for a short period of time compared to the overall duration of the earthquake. Pulse-like rupture requires a time-dependent healing mechanism to arrest slip. In Figure 5 the (a) crack is distinguished from the (b) pulse by the slip rate after the rupture front

has passed, which occurs in the wedge between the pair of expanding fronts. The slip rate relaxes to a steady value for the crack (a lighter shade of blue), and decays to an infinitesimal creeping value for the pulse (a darker shade of blue in the figure). The difference can be difficult to visualize because of the dominant (red) slip rate of the rupture front.

Zheng and Rice [23] found that pulse-like rupture requires low initial shear stress and friction that weakens strongly with slip velocity. The shorter slip duration of pulse-like ruptures are typically accompanied by larger slip rates. The ground motion in earthquakes is sensitive to the slip duration (rise time), which indicates that pulse-like rupture produces ground motion different from a crack-like rupture. Earthquake observations indicate that rupture often occurs in a pulse-like manner [83].

Pulse-like rupture can occur in slip-weakening friction laws in the presence of strong disorder [84, 85]. For example, when a bi-lateral rupture encounters a barrier to rupture (low shear stress or strong frictional properties) in one direction, rupture arrests and sends a healing pulse back towards the other rupture front [86]. These pulse-like ruptures are different from self-healing pulses in that the fault heterogeneity, and not the friction law, are responsible for the arrest of slip.

The speed at which the rupture front propagates along the fault also plays a significant role in the ground motion. The frictional properties of the fault dictate the rupture speed, as an earthquake can rupture through a frictionally weak fault with a large velocity, but a rupture that encounters strong barriers cannot reach as large a velocity.

Rupture speed is important due to the effects of directivity [87], the increase in frequency of ground shaking due to the Doppler effect. Ground motion in the rupture direction has a larger high frequency content. The faster the source is moving along the fault, the larger the Doppler shift, so fast moving ruptures alter the expected ground motion.

A fault with many frictional barriers leads to lower rupture speeds, as the rupture dissipates additional energy to break through the strong patches on a fault. Lower values of the initial stress also slows down ruptures, as less strain energy is released from the elastic bulk. This also decreases the energy that can be radiated as seismic waves, decreasing the intensity of ground shaking. Heterogeneous distributions of friction parameters and the initial stress also influence ground motion. If the strong patches (high frictional resistance or low initial stress) are small and evenly distributed along the fault, the earthquake must break through them in order to rupture the entire fault, and a lower rupture velocity occurs. If the strong patches are grouped together, then the rupture can reach faster rupture speeds by following the large weak patches across the fault [88].

Rupture speed causes significant qualitative and quantitative shifts in ground motion when the rupture exceeds the shear wave speed [89], i.e. supershear ruptures. An example is shown in Figure 5(c). A supershear rupture typically starts out slower than the shear wave speed, and then a second supershear rupture nucleates out ahead of the subshear rupture and propagates faster than the shear wave speed. In Figure 5 (c) the supershear pulses emerge part of the way through the simulation. Faster rupture velocities are associated with the supershear pulse, reflected by the shallower slope in the space vs. time trajectory.

Supershear ruptures only occur for in-plane slip, where the rupture propagation direction and the sense of slip on the fault are identical. In this geometry, ruptures can propagate below the Rayleigh wave speed (slightly less than the shear wave speed), and above the shear wave speed, but not between. Ruptures cannot propagate in this "forbidden" range because energy is not dissipated at the crack tip in these solutions, which is unphysical [89]. Supershear rupture speeds produce shear waves that do not attenuate with distance from the fault [89]. This results in large ground motions significantly further from the fault than for sub-Rayleigh ruptures. Friction laws play a central role in determining if supershear rupture nucleates [90, 91]. Transient increases in rupture velocity to supershear speeds, as opposed to sustained supershear rupture, can also occur due to barriers that require rupture fronts to focus energy on breaking the strong patch [92].

6 Rupture Dynamics with STZ Friction

The remainder of this review follows the implications of microscopic plastic deformation and strain localization for earthquake rupture problems. At the grain scale, the general STZ constitutive equations are developed. The STZ law predicts that for quasi-static, homogeneous deformation the frictional length scale increases with increasing slip rate, which matches observations from laboratory experiments [38]. The STZ law can lead to shear localization, which reduces the frictional length scale, and decreases dynamic sliding friction [46, 47]. These effects are also observed in laboratory experiments [93, 52, 53, 54]. At the fault scale, STZ friction captures the full spectrum of rupture modes, and provides a physical basis for the regimes in which different behaviors may be observed. While this section focuses on strain localization in STZ Theory and its application to relatively simple dynamic rupture problems, in Section 7 we discuss the results in the context of field, laboratory, and numerical studies of faulting and deformation of amorphous materials.

6.1 STZ Friction

The STZ friction model assumes all plastic deformation occurs through STZ rearrangements. STZs switch between two metastable orientations, denoted "positive" and "negative" (see Figure 1). Each switch is accompanied by a fixed increment in the plastic strain. The sign depends on the direction of the orientational shift. Once an STZ has flipped the material cannot shear further in the same direction at that location. Therefore, to accumulate shear the material is constantly creating and destroying STZs as energy is dissipated in the system.

The full STZ model [2, 94, 43] resolves individual populations of positive and negative STZs, including terms for creation and annihilation of STZs, as well as the dynamics of reorientation. For seismic applications the times scales associated with these processes are fast enough to be considered instantaneous, and it is sufficient to model the density of STZs. Energy dissipation in the material drives the density of STZs towards a Boltzmann distribution, with an effective temperature χ, a dimensionless quantity characterizing the configurational disorder in the material. The effective temperature introduced in Equation (4) is normalized by the energy needed to form an STZ divided by Boltzmann's constant to give the dimensionless effective temperature used in the STZ model. Regions with elevated effective temperature are more disordered, have a higher density of STZs, and accommodate more plastic strain.

Quantitatively, STZ theory determines the plastic strain rate $\dot{\gamma}$ in the material based on two factors: χ which determines the number of STZs, and the shear stress τ, which determines how frequently the STZs switch orientation:

$$\dot{\gamma} = f(\tau) \exp(-1/\chi). \tag{5}$$

The stress function $f(\tau)$ has an exponential form [95], which is consistent with laboratory experiments [13]. The exact form in the model is

$$f(\tau) = 2\epsilon/t_0 \exp(-E_0) \cosh(\tau/\sigma_d)(1 - \tau_y/\tau). \tag{6}$$

Other parameters introduced in the stress function are the characteristic strain per STZ reversal ϵ, the STZ rearrangement time scale t_0, the STZ rearrangement activation energy scaled by the STZ formation energy E_0, the STZ activation stress σ_d, and the yield stress τ_y. Below the yield stress, no STZ rearrangements occur, and the plastic strain rate is zero. In the limit of the large stresses of seismic faulting ($\tau >> \sigma_d$), $f(\tau)$ exhibits an approximately exponential dependence on the shear stress.

Effective temperature is different from the thermal temperature, but it evolves in a similar manner. χ obeys a heat diffusion equation which includes terms for energy dissipation, diffusion, and time-dependent relaxation:

$$\frac{\partial \chi}{\partial t} = \frac{\dot{\gamma}\tau}{c_0 \tau_y}\left(1 - \frac{\chi}{\hat{\chi}\left(\dot{\gamma}\right)}\right) + \frac{\partial}{\partial z}\left(\dot{\gamma} D \frac{\partial \chi}{\partial z}\right) + R_0\left(1 - \frac{\chi}{\chi_0}\right)\exp\left(-\beta/\chi\right). \qquad (7)$$

As work is done on the material, dissipation drives the effective temperature towards a steady state $\hat{\chi}(\dot{\gamma})$, and the effective temperature specific heat c_0 determines how rapidly the effective temperature evolves toward steady state. Shearing the material stirs up the particles, and the grains in the system can find higher energy configurations. Only a fraction of the total dissipation increases the effective temperature; the remainder is dissipated as thermal heat [48].

Diffusion of effective temperature is observed in simulations [96], and occurs with a time scale given by the inverse strain rate and a length scale $\sqrt{D}$ determined by the particles in the material. For a granular material, $\sqrt{D}$ is related to the size of the grains. For a glass, $\sqrt{D}$ is determined by the interparticle potential.

Relaxation of χ accounts for time-dependent healing. Here strength recovery is logarithmic in time, as observed in laboratory experiments [97]. Parameters include a relaxation rate R_0, the minimum value to which the effective temperature can relax χ_0, and an effective temperature activation barrier for relaxation β. Time-dependent healing is also important for termination of slip during a dynamic rupture [68, 23] and for fault re-strengthening between earthquakes [98, 99].

The function $\hat{\chi}(\dot{\gamma})$ is based on the observed rate dependence of the steady-state effective temperature in a simulated glass [100]. There are two regimes: at low strain rates, the effective temperature is independent of the strain rate, and at high strain rates the inverse effective temperature depends linearly on the logarithm of the strain rate. Because earthquake rupture occurs at high strain rates, the steady-state effective temperature for dynamic fault slip is always in the rate-dependent regime. This indicates a maximum effective temperature of the form

$$\hat{\chi}\left(\dot{\gamma}\right) = \frac{\chi_w}{\log\left(\frac{q_0}{t_0 \dot{\gamma}}\right)}. \qquad (8)$$

The parameter q_0 determines the dimensionless strain rate at which the effective temperature diverges. At strain rates higher than q_0/t_0, the plastic strain is no longer accommodated as local STZs and instead the deformation is more fluid-like. Simulations provide a quantitative estimate of q_0 [42], and indicate that the effective temperature diverges at a strain rate that is larger than coseismic strain rates.

Therefore, the STZ model is valid at all strain rates in the dynamic rupture simulations.

The parameter χ_w can also be estimated from molecular simulations. Materials with $\chi_w > 1$ are rate strengthening, whereas if $\chi_w < 1$, the steady-state shear stress decreases as the strain rate increases. Rate weakening friction is essential for stick-slip rather than creep dynamics, and so this regime is most relevant for dynamic rupture. However, there are many systems that exhibit rate strengthening behavior, and these materials can form shear bands [44, 45].

6.2 Elastodynamics and STZ Strain Localization

The STZ model captures plastic deformation at the grain and gouge scales, and also acts as a friction law, amenable to investigations of laboratory and seismological instabilities. In simulations, laboratory friction is roughly analogous to a very small fault, comprised of blocks lubricated by interfacial material, and driven by an external shear stress. For most laboratory experiments, the blocks can be modeled as driven by a spring, but otherwise rigid, and sufficiently short that slip occurs coherently (i.e. the entire interface slips at once) rather than as a dynamic rupture which initiates at a nucleation site, and propagates towards the boundaries. The behavior of the STZ friction law is similar for the two cases; instabilities which occur at the onset of slip on the laboratory scale occur at the rupture front during dynamic rupture. We focus on dynamic rupture simulations here. A more detailed analysis of laboratory scale instabilities, including exotic stick-slip patterns, is given in [49].

A detailed illustration of the model fault is shown in Figure 6. The left picture shows a side view of the fault plane. The right picture shows a top view of the fault. A layer of gouge, of half width w, is described by STZ Theory, and is sheared between elastic rock. The inset shows a close up of the fault gouge, where the spatial grid in the z-direction resolves the dynamic evolution of the effective temperature in response to fault slip. In this simplified picture, slip is taken to be a scalar, occurring only in the x-direction, and does not vary with depth (the y-direction). Variations of slip in the x-direction describe dynamic rupture propagation. Variations of slip across the gouge width (the z-direction) describe shear localization. At the laboratory scale, slip only varies in the z-direction.

The elastodynamic response of the surrounding rock is modeled using a boundary integral method [101, 68, 102]. The shear stress $\tau(x,t)$ on the fault is a combination of three terms: the initial shear stress on the fault $\tau_0(x)$, the stress transfer functional $\phi(x,t)$ (the stress change due to the slip on the fault), and radiation damping, which determines the stress change due to instananeous fault slip and depends on the shear

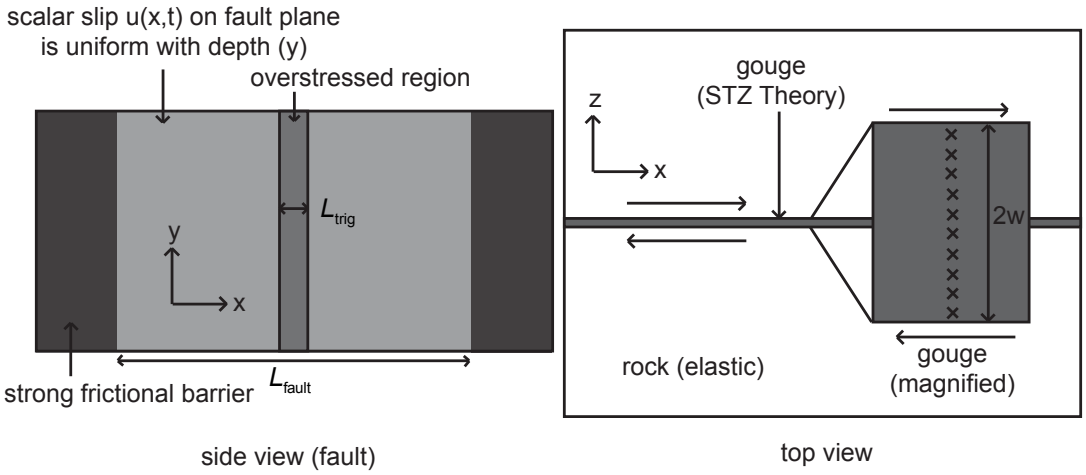

Figure 6: Diagram illustrating the fault in the dynamic rupture model. (left) Side view of the fault plane. Slip is assumed to be uniform with depth. The triggering patch (medium gray) initiates slip, and the rupture spontaneously propagates along strike through the light gray region before it hits the strong barriers (darkest gray) to stop the rupture. (right) Top view of the fault. A thin layer of fault gouge, which is described by STZ Theory, is sheared between elastic rock. Within the fault gouge, a spatial grid resolves the dynamic evolution of the effective temperature across its width (inset). The effective temperature evolves independently at each position along strike, and dynamic fault slip at each point drives the process of strain localization in the model.

modulus G, the shear wave speed c_s, and the slip rate $V(x,t)$:

$$\tau(x,t) = \tau_0(x) + \phi(x,t) - \frac{G}{2c_s}V(x,t). \tag{9}$$

The plastic strain rate integrated across the gouge width gives a second relationship between the shear stress and the slip rate:

$$V = \int_{-w}^{w} \dot{\gamma} dz = f(\tau) \int_{-w}^{w} \exp(-1/\chi)\, dz. \tag{10}$$

Equations (9) and (10) are solved simultaneously for the shear stress and slip rate at every point on the fault, along with the dynamic evolution of the slip and the effective temperature. The initial shear stress is uniform along strike $\tau_0(x) = \tau_0$, with the exception of a triggering patch where the stress is elevated to nucleate rupture. Numerical methods and geophysical parameter estimates are described in detail in Daub *et al.* [47].

The effective temperature initial conditions determine the subsequent evolution of strain rate in the gouge. If the initial effective temperature is spatially uniform across the width of the gouge (z-direction), the rupture is "homogeneous," as in Figure 3(a). If the initial effective temperature includes even a very small spatial perturbation, then the rupture becomes "localized," as in Figure 3(b). In both cases, the strain rate profile varies along strike, as the rupture propagates as in Figure 5. At any given time, there are both spatial points that have not ruptured that still match the initial conditions, as well as points that are actively slipping, where the strain rate profile is determined by the effective temperature evolution.

Strain localization significantly alters the frictional weakening compared to a homogeneous rupture at both laboratory and seismic scales. A plot comparing how stress weakens with slip for a homogeneous rupture and a localized rupture is shown in Fig. 7(a). Here the initial conditions for effective temperature include a small perturbation for the localized case, and the shear band width evolves to 10% of the total gouge width $2w$ during slip. During the initial stages, the shear stress for homogeneous and localized cases are nearly indistinguishable. However, after roughly 0.01 m of slip, there is a dramatic drop in the friction for the localized case, and the interface weakens much more rapidly due to the dynamic instability of localization. Homogeneous deformation and dynamic localization produce very different slip rates, as can be seen in Fig. 7(b). The rupture front arrives earlier and has a higher peak slip rate when strain localization occurs.

Different shear band thicknesses form for localized ruptures with different diffusion length scales. Shear band thicknesses ranges from broad shear bands that fill

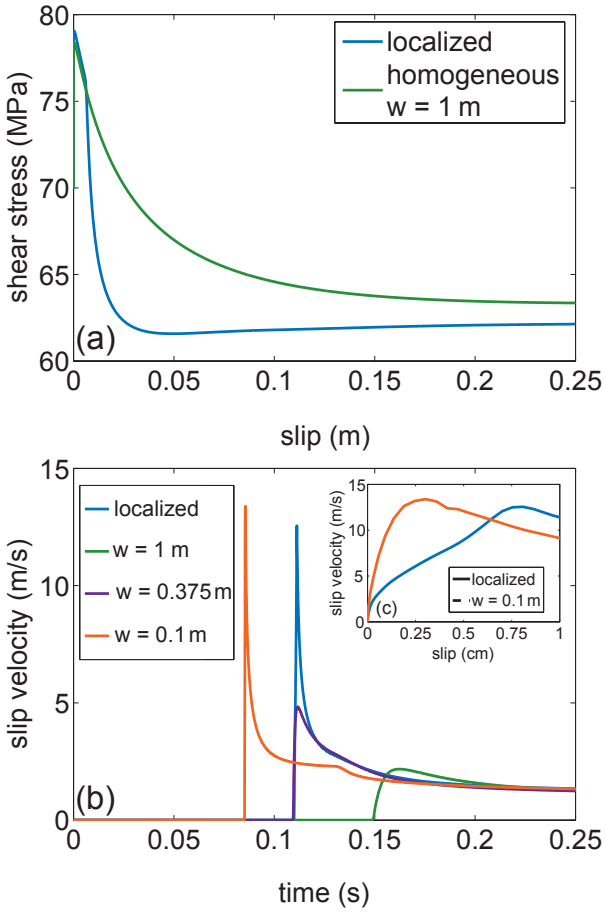

Figure 7: Dynamic rupture evolution at a point 0.35 km from the hypocenter in an expanding crack. (a) Comparison of shear stress as a function of slip shows a sharp weakening in the localized case. (b) Slip rate as a function of time. Localized rupture is compared with a host of models with varying gouge width w and homogeneous strain, none of which can match both the peak slip rate and rupture front arrival of the localized case. (c) Inset: Slip rate as a function of slip for the localized and narrowest width homogeneous rupture.

the gouge layer to shear bands that are much narrower than the gouge width. The distinction between broad and narrow shear bands is important because localization is a mechanism for dynamic weakening. The narrower the shear band, the larger the strain rate in the shear band, and the lower the shear stress.

To illustrate the importance of the dynamic instability, results for localized shear are compared with two additional homogeneous ruptures of different fixed gouge widths w chosen to match particular aspects of the localized rupture. Slip velocity as a function of time is plotted at a point 0.35 km from the hypocenter for all models in Fig. 7(b). The rupture front in the intermediate model ($w = 0.375$ m) matches the arrival time of the localized rupture, but the peak slip rate is smaller. For the narrowest gouge thickness ($w = 0.1$ m), peak slip rates may be similar to the localized rupture but the rupture arrives earlier. Figure 7(c) plots the slip rate as a function of slip distance for the homogeneous rupture with $w = 0.1$ m and the localized rupture. This clearly shows that the initial broad deformation in the localized rupture does not simply delay the rupture, but also lessens the slip acceleration during the earliest stages of slip. No homogeneous rupture can mimic the macroscopic effects of the internal dynamical instability that produces localization.

6.3 Internal Dynamics of Localization

The small scale effective temperature dynamics of localization in the gouge are intimately connected with macroscopic stress and strain during dynamics rupture. This is illustrated for a pulse-like rupture in Figure 8 for a particular point along the fault, 2 km from the hypocenter. A plot of shear stress as a function of slip is shown in Figure 8 (a). As the rupture passes through, the shear stress weakens in two distinct phases. For slip less than 0.1 m, stress weakens gradually with slip. This phase is described by a nearly spatially uniform effective temperature, and occurs before the shear band is well defined. For slip between 0.1 m and 0.3 m, the stress drops sharply due to the rapid growth of the shear band. The stress weakens to a minimum and then increases. Slip stops shortly before 0.7 m, and the fault heals. In contrast, Figure 7 is generated using different parameters corresponding to an expanding crack, so there is not a significant increase in stress at the later stages of slip, but the internal evolution of effective temperature during the initial weakening phase is similar.

In Figure 8 (b) snapshots of the effective temperature across the gouge width are shown at the sequential stages marked on the stress versus slip curve (Figure 8 (a)). The earliest effective temperature plot shows that during the initial weakening phase of the stress versus slip curve, the gouge deforms approximately homogeneously.

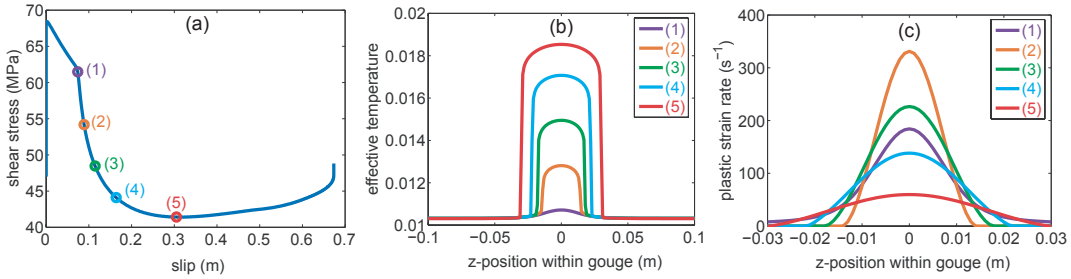

Figure 8: Dynamics of slip and localization for a self-healing pulse with $\sqrt{D}/w = 0.2236$ and $\tau_0 = 47$ MPa. All plots are at a point on the fault 2 km from the hypocenter. (a) Shear stress as a function of slip. (b) Effective temperature as a function of z-position within the gouge at representative points shown in (a). The horizontal range in this plot shows the entire gouge width in the simulation. (c) Plastic strain rate as a function of position within the gouge at representative points shown in plot (a). Note that the horizontal range in this plot is smaller than in plot (b).

However, as slip progresses any perturbation to the effective temperature spontaneously grows as the gouge is sheared due to a feedback in the effective temperature evolution law. The energy dissipation term in Equation (7) is proportional to the strain rate, so the effective temperature at a point with an elevated effective temperature grows more rapidly than others. This feeds back into the dissipation term, and leads to strain localization and the formation of a shear band [45, 47]. Feedbacks in the effective temperature equation require time to amplify heterogeneity in the initial conditions. The duration of the initial phase of weakening is controlled by the magnitude of the initial perturbation to the effective temperature. Larger initial perturbations require less time to dynamically grow and shorten the amount of slip before the shear band forms. The onset of rapid weakening for the localized case in Figure 7 occurs over a smaller slip distance compared to Figure 8, due to a small difference in the amplitude of the initial effective temperature perturbation.

As the successive plots of the effective temperature show, the effective temperature in the shear band grows rapidly in magnitude, and the width of the shear band increases as the stress on the fault drops. The expanding width is due to the diffusion of effective temperature. The shear band reaches its maximum width when the stress reaches its minimum value, and the same shear band width is maintained for the duration of slip.

The strain rate is locally higher in the shear band, and the friction weakens with

strain rate, so the shear stress while sliding with a shear band is lower than for the case without a shear band. The rapid weakening of the shear stress at the initial stages of shear band formation coincides with the largest strain rates during rupture, as illustrated in Figure 8(c). This is because shear stress decreases most rapidly with slip at this time, releasing the most strain energy from the bulk. Subsequently, the strain rate at the center of the gouge decreases as the stress continues to drop with further slip, and the shear band broadens due to diffusion of the effective temperature.

Manning *et al.* [45] showed that for rate weakening parameters, any perturbation to the initial effective temperature grows unstably as the material is sheared. For rate strengthening materials, the STZ equations are linearly stable to perturbations to the effective temperature. However, shear bands can still form due to transient effects. Strain localization is observed in rocks below the seismogenic zone [103] where frictional behavior is believed to be rate strengthening [22], and simulations with STZ Theory show that dynamic rupture propagating below the seismogenic zone produces this transient localization [104].

6.4 STZ Fault Scale Rupture

The rupture type– crack, pulse, or supershear– depends on both the initial shear stress on the fault and the dynamic evolution of friction. Strain localization decreases frictional dissipation and is a mechanism for dynamic weakening, and both these effects influence the spatiotemporal propagation of slip in an earthquake. The diffusion length scale $\sqrt{D}$ controls the degree of localization. Small values of the diffusion constant produce narrow shear bands, while larger values of the diffusion constant produce broad shear bands. An order of magnitude variation in the diffusion length scale $\sqrt{D}$ produce a range of shear bands ranging from the full width of the gouge ($\sqrt{D} = w$) down to much narrower shear bands ($\sqrt{D} = 0.1w$).

The effect of the initial shear stress and the shear band width on fault scale rupture is illustrated in Figure 9. For each value of the initial stress and each value of the diffusion constant, a corresponding point can be located on the plot identifying the rupture type that occurs in a dynamic rupture simulation. The diagram includes the rupture types shown in Figure 5(a)-(c), as well as pulse-like and crack-like ruptures that arrest before rupturing the entire fault due to a low initial shear stress.

As expected, the additional weakening and reduced frictional dissipation for the more localized ruptures reduces the minimum shear stress for all types of rupture. The upper curve in Figure 9 is the minimum stress needed to nucleate supershear rupture. An order of magnitude reduction in the diffusion constant reduces the minimum stress needed to nucleate supershear rupture by about 7 MPa, a significant

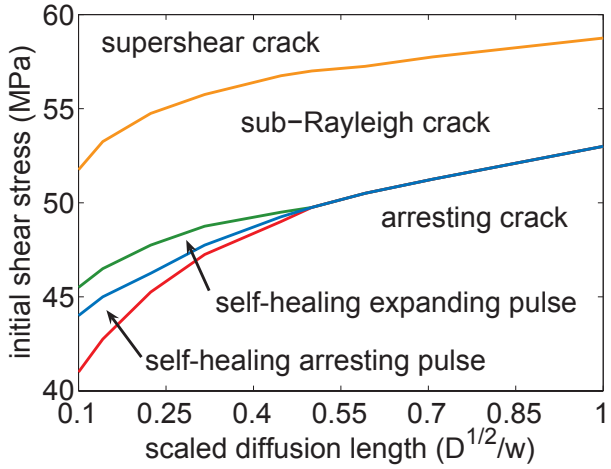

Figure 9: Rupture classification diagram as a function of diffusion length scale and initial shear stress for ruptures with STZ Theory.

fraction of the initial shear stress on the fault.

The lower curves in Figure 9 indicate how localization affects rupture propagation at lower initial shear stress. For broad shear bands, slip can only grow in a crack-like manner, but as the diffusion constant is decreased, pulse-like rupture can occur. This is because localization leads to additional dynamic weakening, which was shown to be the crucial frictional characteristic determining when slip propagates as a self-healing pulse by Zheng and Rice [23]. The solid line marks the lowest stress required to propagate slip over the entire fault. This involves crack-like rupture if $\sqrt{D} > 0.5w$ and pulse-like rupture if $\sqrt{D} < 0.5w$. The initial stress needed to fully rupture the fault decreases by nearly 10 MPa, a significant fraction of the initial shear stress.

7 Discussion

In the STZ model, shear bands spontaneously form and grow in response to dynamic rupture. This provides a unique description of fault friction based on the dynamic evolution of the effective temperature. Strain localization increases both the stress drop and peak slip rate. Ground motion away from the fault tends to be larger if the peak slip rate is increased [105], which suggests that strain localization may impact the ground motion in real earthquakes.

Localization plays an important role in determining rupture propagation speed and type, features that can qualitatively alter estimates for ground motion. Localiza-

tion provides the dynamic weakening necessary for pulse-like rupture and significantly reduces the minimum initial stress for the earthquake to rupture the entire fault. Seismic observations suggest pulse-like rupture propagation in many earthquakes [83], and the dynamic weakening provided by localization may play an important role in producing pulse-like rupture. Supershear ruptures radiate seismic waves with a distinct attenuation pattern compared to sub-Rayleigh ruptures [89]. There is evidence of supershear rupture speeds in many earthquakes [106, 107, 108, 109, 110], as well as observations of supershear rupture in laboratory slip experiments [111]. In the STZ results presented here, the stress which marks the transition to supershear changes by a significant amount for the narrowest shear bands.

Slip surfaces are often observed at the boundary between gouge and the host rock in both exhumed faults [61] and laboratory experiments [52]. In STZ Theory, the position where the shear band forms depends on where the initial effective temperature is largest. If there are two or more positions with an equally large initial effective temperature, strain localizes to one. If one of the possible locations is at the boundary, the shear band prefers to form at the boundary rather than in the interior of the gouge layer. Boundary conditions on the effective temperature may also play a role. The results reported here use no conduction boundary conditions, but other boundary conditions, such as fixed effective temperature at the boundary, may yield different results for the preferred shear band location.

The underlying physical basis of the STZ friction law provides an opportunity to connect atomistic and granular numerical simulations with laboratory experiments and seismic observations by varying the fundamental parameters in the theory. Varying the effective temperature diffusion length scale determines how the amount of dynamic weakening impacts the propagation of ruptures. The final shear band width that the material chooses is dynamically selected by a balance between the nonlinear processes of energy dissipation, effective temperature diffusion, and healing. The width is proportional to the diffusion length scale $\sqrt{D}$, but it also depends on the stress, the effective temperature, and the effective temperature specific heat [49].

Simulations, experiments, and field observations yield a wide range of shear band thicknesses in amorphous materials. Simulations of glassy materials indicate that shear band thicknesses tend to be approximately 10 particle diameters [2], though for granular materials this could be very different because particles have a greater variety of sizes. Morgan and Boettcher [51] determined that deformation in numerical simulations of fault gouge tends to localize to a narrower shear band when a particle size distribution more heavily weighted towards small particles is used. In each of their simulations, the shear band is only a few particle diameters wide. However, simulations do not include the full range of particle sizes that are found in natural

faults [112]. Experimental investigations of granular materials indicate that shear band thickness scales with the "mean particle diameter," defined such that 50% of the particles by weight have larger size [113]. Rock mechanics studies on laboratory faults with gouge observe shear band thicknesses that depend on the grain sizes, with the shear band thicknesses ranging from around 100 μm [52] to several millimeters [55].

In exhumed faults slip surfaces range from hundreds of microns to a few millimeters, even narrower than the shear bands in the simulations presented here [60, 61, 62], indicating that the dynamic weakening from strain localization could be even more dramatic. Computational limits restrict the range of diffusion lengths that can be considered – the effective temperature grid must be fine enough to resolve the shear band, and the narrower shear bands reduce the slip scale over which the stress weakens. This rapid stress drop requires a smaller grid spacing along strike to produce well resolved simulations.

Core samples from the creeping section of the San Andreas Fault Observatory at Depth (SAFOD) indicate that slip occurs throughout the entire gouge width of about 2-3 m (i.e. not localized within the layer) [64]. Laboratory experiments with gouge from the creeping section indicate rate strengthening friction parameters [114]. These results are consistent with STZ Theory, which predicts that rate strengthening materials form shear bands only as transient phenomena [45]. When a rate strengthening material is loaded at a relatively constant rate, STZ Theory predicts that steady sliding is stable and deformation is accomodated over the entire width of the fault gouge, in agreement with the SAFOD experiment.

STZ Theory provides a microscopic physical basis for plastic deformation in fault gouge. There are also many other processes that are important during seismic slip which are likely to couple to the STZ dynamics, and are not yet incorporated into STZ Theory. This includes brittle fracture, wear, and comminution, which create the finely grained gouge in the fault zone [112], and thermal heating and weakening, melting, and pressurization of fluids are also believed to be important during fault slip [33, 26, 27, 29, 30]. These processes likely influence the rate at which STZs reverse and how the effective temperature evolves. Determining how these additional processes couple to the STZ friction law may provide further constraints on the physics of the earthquake source.

Acknowledgements: This work was supported by NSF Grant Number DMR-0606092, the NSF/USGS Southern California Earthquake Center, funded by NSF Cooperative Agreement EAR-0106924 and USGS Cooperative Agreement 02HQAG0008, and the David and Lucile Packard Foundation.

References

[1] Falk ML, Shi Y. 2002. In *Supercooled Liquids, Glass Transition, and Bulk Metallic Glasses. Mat. Res. Soc. Symp. Proc.*, vol. 754, edited by T. Egami et al. p. 257. Warrendale, Pa.

[2] Falk ML, Langer JS. 1998. *Phys. Rev. E* 57(6):7192-7205.

[3] Ida Y. 1972. *J. Geophys. Res.* 77(20):3796-3805.

[4] Andrews DJ. 1976.*J. Geophys. Res.* 81:3575-3582.

[5] Andrews DJ. 1976. *J. Geophys. Res.* 81:5679-5687.

[6] Ohnaka M. 2003. *J. Geophys. Res.* 108(B2):2080.

[7] Palmer AC, Rice JR. 1973. *Proc. R. Soc. London, Ser. A* 332:527-548.

[8] Day SM. 1982. *Bull. Seismol. Soc. Am.* 72:1881-1902.

[9] Harris RA, Day SM. 1993. *J. Geophys. Res.* 98:4461-4472.

[10] Madariaga R, Olsen KB, Archuleta RJ. 1998. *Bull. Seismol. Soc. Am.* 88:1182-1197.

[11] Blau, P. J. (1989), in *Friction and Wear Transitions of Materials: Break- in, Run-in, Wear-in*, Noyes, Park Ridge, NJ, 312-317.

[12] Rice JR, Ruina AL. 1983. *J. Appl. Mech.* 50:343-349.

[13] Dieterich JH. 1979. *J. Geophys. Res.* 84(NB5):2161-2168.

[14] Ruina AL. 1980. *Friction laws and instabilities: A quasistatic analysis of some dry frictional behavior*. Ph.D. Thesis, Brown University, Providence, R.I.

[15] Ruina AL. 1983. *J. Geophys. Res.* 88:10359-10370.

[16] Dieterich JH, Kilgore BD. 1994. *Pure Appl. Geophys.* 143(1-3):283-302.

[17] Kato N, Tullis TE. 2001. *Geophys. Res. Lett.* 28(6):1103-1106.

[18] Rice JR. 1983. *Pure Appl. Geophys.* 121:443-475.

[19] Stesky RM, Brace WF, Riley DK, Robin PYF. 1974. *Tectonophysics* 23(1-2):177-203.

[20] Blanpied ML, Lockner DA, Byerlee JD. 1991. *Geophys. Res. Lett.* 18(4):609-612.

[21] Blanpied ML, Lockner DA, Byerlee JD. 1995. *J. Geophys. Res.* 100(B7):13,045-13,064.

[22] Scholz CH. 1998. *Nature* 391:37-42.

[23] Zheng G, Rice JR. 1998. *Bull. Seismol. Soc. Am.* 88:1466-1483.

[24] Favreau P, Ionescu IR, Campillo M. 1999. *Geophys. J. Int.* 139(3):671-678.

[25] Rice JR, Lapusta N, Ranjith K. 2001. *J. Mech. Phys. Solids* 49:1865-1898,

[26] Tullis TE, Goldsby DL. 2003. *Eos Trans. AGU* 84(46), Fall Meet. Suppl., Abstract S51B-05.

[27] Di Toro G, Goldsby DL, Tullis TE. 2004. *Nature* 427:436-439.

[28] O'Hara K, Mizoguchi K, Shimamoto T, Hower JC. 2006. *Tectonophysics* 424:109-118.

[29] Di Toro G, Hirose T, Nielsen S, Pennacchioni G, Shimamoto T. 2006. *Science* 311:647-649.

[30] Rice JR. 2006. *J. Geophys. Res.* 111:B05311.

[31] Hirose T, Shimamoto T. 2005. *J. Geophys. Res.* 110(B5):B05202.

[32] Tsutsumi A, Shimamoto T. 1997. *Geophys. Res. Lett.* 24(6):699-702.

[33] Lachenbruch AH. 1980. *J. Geophys. Res.* 85(NB11):6097-6112.

[34] Hickman SH. 1991. *Rev. Geophys.* 29:759-775.

[35] Sibson RH. 1994. In *Faulting, Friction and Earthquake Mechanics*, Part 1, pp. 645-662. Birkhaeuser Verlag, Basel, Switzerland.

[36] Kanamori H, Heaton TH. 2000. In *Geocomplexity and the Physics of Earthquakes*, American Geophysical Union Geophysical Monograph 120, pp. 147-163. AGU, Washington, DC.

[37] Lapusta N, and Rice JR. 2003. *Eos Trans. AGU* 84(46), Fall Meet. Suppl., Abstract S51B-02.

[38] Daub EG, Carlson JM. 2008. *J. Geophys. Res.* 113:B12309.

[39] Noda H, Dunham EM, Rice JR. 2009. *J. Geophys. Res.* 114:B07302.

[40] Falk ML, Langer JS. 2000. *MRS Bull.* 25(5):40-45.

[41] Lois G, Lemaitre A, Carlson JM. 2005. *Phys. Rev. E* 72:051303.

[42] Haxton TK, Liu AJ. 2007. *Phys. Rev. Lett.* 99:195701.

[43] Lemaitre A, Carlson JM. 2004. *Phys. Rev. E* 69(6):061611.

[44] Manning ML, Langer JS, Carlson JM. 2007. *Phys. Rev. E* 76(5):056106.

[45] Manning ML, Daub EG, Langer JS, Carlson JM. 2009. *Phys. Rev. E* 79:016110.

[46] Daub EG, Manning ML, Carlson JM. 2008. *Geophys. Res. Lett.* 35:L12310.

[47] Daub EG, Manning ML, Carlson JM. submitted to *J. Geophys. Res.*.

[48] Hermunstad AM, Daub EG, Carlson JM. Submitted to *J. Geophys. Res.*

[49] Daub EG, Carlson JM. Submitted to *Phys. Rev. E*.

[50] Langer JS. 2008. *Phys. Rev. E* 77:021502.

[51] Morgan JK, Boettcher MS. 1999. *J. Geophys. Res.* 104(B2):2703-2720.

[52] Beeler NM, Tullis TE, Blanpied ML, Weeks JD. 1996. *J. Geophys. Res.* 101(B4):8697-8715.

[53] Marone C. 1998. *Ann. Rev. Earth Planet. Sci.* 26:643-696.

[54] Mair K, Marone C. 1999. *J. Geophys. Res.* 104(B12):28899-28914.

[55] Chambon G, Schmittbuhl J, Corfdir A. 2006. *J. Geophys. Res.* 111:B09308.

[56] Lu J, Ravichandran G, Johnson WL. 2003. *Acta Mater.* 51(12):3429-3443.

[57] Tsai JC, Gollub JP. 2005. *Phys. Rev. E* 72:051304.

[58] Lauridsen J, Twardos M, Dennin M. 2002. *Phys. Rev. Lett.* 89:098303.

[59] Daniels KE, Hayman NW. 2008. *J. Geophys. Res.* 113:B11411.

[60] Chester FM, Evans JP, Biegel RL. 1993. *J. Geophys. Res.* 98(B1):771-786.

[61] Chester FM, Chester JS. 1998. *Tectonophysics* 295:199-221.

[62] Wibberley CAJ, Shimamoto T. 2003. *J. Struct. Geol.* 25(1):59-78.

[63] Zoback MD. 2006. *Scientific Drilling* 2(2006):32-33.

[64] Hickman SH, Zoback MD, Ellsworth WL, Kirschner D, Solum J. 2007. *Eos Trans. AGU*, 88(52) Fall Meet. Suppl. Abstract T44B-01.

[65] Okubo P. 1989. *J. Geophys. Res.* 94(B9):12321-12335.

[66] Bizzarri A, Cocco M. 2003. *J. Geophys. Res.* 108(B8):2373.

[67] Cocco M, Bizzari A. 2002. *Geophys. Res. Lett.* 29(11):1516.

[68] Perrin G, Rice JR, Zheng G. 1995. *J. Mech. Phys. Solids* 43:1461-1495.

[69] Harris RA. 2004. *Pure Appl. Geophys.* 161(11-12):2171-2181.

[70] Olsen KB, Madariaga R, Archuleta RJ. 1997. *Science* 278:834-838.

[71] Page MT, Dunham EM, Carlson JM. 2005. *J. Geophys. Res.* 110:B11302.

[72] Nielsen SB, Carlson JM, Olsen KB. 2000. *J. Geophys. Res.* 105(B3):6069-6088.

[73] Nielsen SB, Carlson JM. 2000. *Bull. Seismol. Soc. Am.* 90:1480-1497.

[74] Bizzarri A, Cocco M, Andrews DJ, Boschi E. 2001. *Geophys. J. Int.* 143(3):656-678.

[75] Bizzarri A, Cocco M. 2005. *Annals of Geophys.* 48(2):279-299.

[76] Guatteri M, Spudich P. 2000. *Bull. Seism. Soc. Am.* 90:98-116.

[77] Carlson JM, Langer JS. 1989. *Phys. Rev. A* 40:6470.

[78] Cochard A, Madariaga R. 1996. *J. Geophys. Res.* 101:25321-25336.

[79] Shaw BE, Rice JR. 2000. *J. Geophys. Res.* 105(B10):23791-23810.

[80] Lapusta N, Rice JR, Ben-Zion Y, Zheng G. 2000. *J. Geophys. Res.* 105(B10):23765-23789.

[81] Lapusta N, Rice JR. 2003. *J. Geophys. Res.* 108(B4):2205.

[82] Kostrov B. 1964. *J. Appl. Math. Mech.* 28:1077-1087.

[83] Heaton TH. 1990. *Phys. Earth Plant. Int.* 64(1):1-20.

[84] Beroza G, Mikumo T. 1996. *J. Geophys. Res.* 101:22449-22460.

[85] Ide S, Takeo M. 1997. *J. Geophys. Res.* 102(B12):27379-27391.

[86] Day SM. 1982. *Bull Seismol. Soc. Am.* 72:705-727.

[87] Das S, Kostrov BV. 1983. *J. Geophys. Res.* 88:4277-4288.

[88] Schmedes J, Archuleta RJ, Lavallée D. Submitted to *J. Geophys. Res.*

[89] Dunham EM, Archuleta RJ. 2005. *Geophys. Res. Lett.* 32(3):L03302.

[90] Dunham EM. 2007. *J. Geophys. Res.* 112:B07302.

[91] Schmedes J, Archuleta RJ, Lavallée D. 2009. *Seismol. Res. Lett.* 80(2):301.

[92] Dunham EM, Favreau P, Carlson JM. 2003. *Science* 299:1557.

[93] Marone C, Kilgore B. 1993. *Nature* 362(6421):618-621.

[94] Lemaitre A. 2002. *Phys. Rev. Lett.* 89(19):195503.

[95] Eyring HJ. 1936. *J. Chem. Phys.* 4:283.

[96] Shi Y, Katz MB, Li H, Falk ML. 2007. *Phys. Rev. Lett.* 98:185505.

[97] Dieterich JH. 1972. *J. Geophys. Res.* 77(20):3690.

[98] Marone CJ, Vidale JE, Ellsworth WL. 1995. *Geophys. Res. Lett.* 22(22):3095-3098.

[99] Li YG, Vidale JE, Day SM, Oglesby DD, Cochran E. 2003. *Bull. Seismol. Soc. Am* 93:854-869.

[100] Langer JS, Manning ML. 2007. *Phys. Rev. E* 76:056107.

[101] Cochard A, Madariaga R. 1994. *Pure Appl. Geophys.* 142(3-4):419-445.

[102] Geubelle PH, Rice JR. 1995. *J. Mech. Phys. Solids* 43(11):1791-1824.

[103] Simpson C. 1984. *Geology* 12(1):8-11.

[104] Daub EG. 2009. *Deformation and Localization in Earthquake Ruptures and Stick-Slip Instabilities*. PhD Thesis. Univ, Calif., Santa Barbara. 242 pp.

[105] Aagaard BT, Hall JF, Heaton TH. 2001. *Earthquake Spectra* 17:177-207.

[106] Archuleta RJ. 1984. *J. Geophys. Res.* 89:4559-4585.

[107] Bouchon M, Bouin MP, Karabulut H, Toksöz MN, Dietrich M, Rosakis A. 2001. *Geophys. Res. Lett.* 28(14):2723-2726.

[108] Bouchon M, Vallée M. 2003.*Science* 301:824-826.

[109] Ellsworth WL, Celebi M, Evans JR, Jensen EG, Kayen R, et al. 2004. *Earthquake Spectra* 20(3):597-615.

[110] Dunham EM, Archuleta RJ. 2004. *Bull. Seismol. Soc. Am.* 94(6):256-268.

[111] Rosakis AJ, Samudrala O, Coker D. 1999. *Science* 284:1337-1340.

[112] Chester JS, Chester FM, Kronenberg AK. 2005. *Nature* 437:133-136.

[113] Tordesillas A, Peters JF, Gardiner BS. 2004. *Int. J. Numer. Anal. Methods Geomech.* 28:981-1010.

[114] Carpenter BM, Marone CJ, Saffer DM. 2009. *Geophys. Res. Lett.* 36:L05302.